Investigating future changes in the volume budget of the Arctic sea ice in a coupled climate model

Ann Keen[1] and Ed Blockley[1]

[1]Met Office, FitzRoy Road, Exeter, EX1 3PB, United Kingdom

5 *Correspondence to*: Ann Keen (ann.keen@metoffice.gov.uk)

Abstract. We consider the volume budget of the Arctic sea ice in the CMIP5 global coupled model HadGEM2-ES, and evaluate how the budget components evolve during the 21st century under a range of different forcing scenarios. As the climate warms and the ice cover declines, the Arctic sea ice processes that change the most in HadGEM2-ES are summer melting at the top surface of the ice, and basal melting due to extra heat from the warming ocean. However, the declining ice

10 cover affects how much impact these changes have on the ice volume budget, where the biggest contribution to Arctic ice decline is the reduction in the total amount of basal ice formation during the autumn and early winter. This highlights the importance of taking the declining ice area into account when evaluating projected changes in the sea ice budget, especially if comparing models with very different rates of decline.

Changes in the volume budget during the 21st century have a distinctive seasonal cycle, with processes contributing to ice

15 decline occurring in May/June and September to November. During July and August the total amount of sea ice melt decreases, due to the reducing ice cover.

The choice of forcing scenario affects the rate of ice decline and the timing and magnitude of changes in the volume budget components, but for the HadGEM2-ES model and for the range of scenarios considered for CMIP5, the mean changes in the volume budget depend on the evolving ice area, and are independent of the speed at which the ice cover declines.

1 Introduction

Arctic September sea ice cover has declined at a rate of over 13% per decade since satellite observations began (Serreze and Stroeve, 2015), and the ice that remains is becoming thinner (Kwok and Rothrock, 2009), younger (Maslanik et al, 2011),

25 and faster moving (Rampal et al, 2009, Spreen et al, 2011). The ice cover is projected to reduce further as greenhouse gas concentrations continue to increase (Stroeve et al, 2012). These changes have implications both within the Arctic itself, for example for shipping (Melia et al, 2016), and local ecology (Post et al, 2013), and also for the wider climate system via large scale circulation changes that have been linked to the reducing Arctic ice cover (Francis et al 2009, Overland and Wang,

2010). As the sea ice interacts directly with both the atmosphere and the ocean, it is influenced by changes in both, and as such can be seen as an integrator of wider changes within the Arctic region.

Hence there is much interest in how the decline in Arctic sea ice will continue in the future, both in terms of the predictability of ice cover in a given year, and in terms of the manner and timing of the transition to a seasonally ice-free
5   Arctic. Global coupled models are arguably the best tool we have for making future projections of the Arctic sea ice, but generate a wide spread of projections of future ice decline (Stroeve et al 2012).   There are many factors potentially contributing to this spread, including sea ice model formulation, forcing from atmosphere and ocean model components, uncertainty in forcing scenarios, and internal model variability. A number of studies have attempted to decrease the spread of plausible future projections by sub-selecting models based on their ability to simulate current day sea ice (Wang and
10   Overland, 2009), or past observed changes (Massonnet et al, 2012). More recent work has focussed on the role of internal model variability (Jahn et al, 2016), and the extent to which it is realistic to expect modelled ice decline to closely match the observed decline (Notz, 2015).

Given the inherent uncertainties in predicting future changes in 'integrated' quantities like ice cover and volume, it is becoming increasingly clear that it is also necessary to consider, compare and evaluate the underlying processes causing ice
15   growth and decline, and how they are likely to change in a warming world. Holland et al (2010) evaluated the annual mean changes in ice growth, melt and divergence during the 21st century for a range of models submitted to the CMIP3 model archive, finding considerable variation in the magnitude and relative importance of changes in the budget components. For this 2010 study, the budget components were derived from model monthly ice thickness and velocity from the CMIP3 data archive. However for individual models a more detailed decomposition is often possible (eg Keen et al, 2013), and for
20   CMIP6 models a wide range of budget components should be available for intercomparison (Notz et al, 2016). In addition, new process-based observational datasets are becoming available to help understand whether the modelled ice state arises for the right reasons (Holland and Kimura, 2016, Uotila et al, 2014).

In this study we consider the processes contributing to 21st century changes in the volume of the Arctic sea ice and overlying
25   snow in the Met Office Hadley Centre Earth system model HadGEM2-ES (Martin et al. 2011; Collins et al. 2011), which was one of the models submitted to the IPCC AR5 assessment. We consider a volume budget decomposition similar to that previously used by Keen et al (2013) for the HadGEM1 model, to identify how the components of the budget change during the 21st century under a range of future emissions scenarios, and which components play the most important role in the decline in ice volume. In Sect. 2 we describe the model and the forcing scenarios used. In Sect. 3 we describe the mean
30   volume budget for this model, and in Sect. 4 we investigate how this changes during the 21st century for a range of forcing scenarios. In Sect. 5 we summarise and discuss our findings.

2 Model description and integrations used

2.1 Model description

HadGEM2-ES is a coupled atmosphere-ocean model that was submitted to CMIP5 for use in IPCC AR5. The model includes interactive atmosphere and ocean carbon cycles, dynamic vegetation, and tropospheric chemistry (Martin et al.

5 2011; Collins et al. 2011). HadGEM2-ES is considered to have a good depiction of present-day global cloud characteristics (Jiang et al, 2012) and the best model depiction of Arctic cloud and surface radiative forcing (English et al 2015). The mean Arctic ice extent lies within 20% of observed values at all time of year, although September extent is biased low and the magnitude of the seasonal cycle is too large, consistent with biases in winter net surface LW and summer net surface SW (West et al, 2017)

10 The horizontal resolution of the atmosphere component is 1.25° latitude by 1.875° longitude, with 38 vertical levels. The ocean component is 1° by 1° outside the tropics, increasing to 0.33° latitude by 1° longitude at the equator, and has 40 vertical levels. The sea ice formulation within HadGEM2-ES is essentially the same as that used in HadGEM1 (McLaren et al., 2006), with three updates as follows:

- The bare sea ice albedo was increased from 0.57 to 0.61, together with a correction to sea-ice albedo during surface
15 melt.

- Heat fluxes passed from the atmosphere to the ocean/seaice model are regridded taking the ice concentration into consideration.

- Sea ice velocities are combined with ocean currents to create a "surface velocity" field for use in the atmosphere model.

20 Some of the sea ice calculations take place within the atmosphere component, where the sea ice surface temperature and the top melting and diffusive heat fluxes are computed using the zero-layer thermodynamics scheme described by Semtner (1976). In this scheme the sea ice has no heat capacity, and the ice and any overlying snow are treated as one layer with an effective thickness h_e defined as

$$h_e = h + (\kappa_i/\kappa_s)h_s \tag{1}$$

25 where h is the ice thickness, κ_i and κ_s are the (constant) thermal conductivities of ice and snow, and h_s is the snow depth. The albedo of the sea ice is a function of surface temperature (Curry et al, 2001), allowing the radiative impact of melt ponds to be represented in a simple way.

The growth and melt of ice is calculated within the ocean component, and the ocean to ice heat flux is calculated following McPhee (1992). There is a sub-gridscale ice thickness distribution (Thorndike et al, 1975), with 5 thickness categories plus

30 open water, and the thermodynamic transfer of ice between categories is calculated using a linear remapping scheme (Lipscomb, 2001). Ice velocities are calculated following the elastic-viscous-plastic (EVP) model of Hunke and Dukowicz (1997), using the Hibler (1979) formulation for ice strength. The amount of ridging is determined following the approach used in the CICE model (Lipscomb and Hunke, 2004). For a fuller description of the HadGEM1 sea ice component, see

McLaren et al (2006).

2.2 Model integrations

The integrations used here are described in Jones et al (2011), and include an ensemble of 4 historical simulations (Hist) using observed forcing from 1860 to 2005, and initialised from the model state at 50 year intervals of a pre-industrial control

5   integration. Four different climate forcing scenarios developed for the IPCC Fifth Assessment Report (AR5) (Moss et al, 2010), were then run from the end of each of these historical simulations:

- Representative Concentration Pathway (RCP) 2.6: A low emissions scenario, with CO_2 concentration levelling off, and then starting to decline towards the end of the century.

- RCP4.5: A medium forcing scenario, in which the forcing stabilises during the latter part of the 21st century.

10   - RCP6.0: Another medium forcing scenario, but in this case the forcing continues to increase throughout the 21st century.

- RCP8.5: A strong forcing scenario, with ongoing increases in CO_2 concentration throughout (and beyond) the 2[1st] century.

Figure 1a of Caesar et al (2012) shows the prescribed CO_2 concentrations for each of these scenarios. Here we consider the

15   period 1960 to 2099 (comprising part of the historical period, followed by the scenario), and Fig. 1 shows the global temperature anomalies for these HadGEM2-ES integrations w.r.t. a reference period taken as the years 1960-79. There is little divergence in the global temperature response before the middle of the 21st century, but by 2100 the temperature increase relative to 1960-79 ranges from less than 2 degrees for RCP2.6 to nearly 6 degrees for RCP8.5.

2.3 Evolution of ice area and volume

20   We focus on changes in the sea ice over the domain shown in Fig. 2, covering the Arctic basin, and the Barents Sea. Figure 3 shows how the ice area and the volume of ice and snow within this domain declines for each of the model integrations during the period 1960 to 2090. The ice volume includes the impact of any overlying snow by converting the snow to an equivalent volume of ice using Eq. (1). This effective ice volume is expressed as a mean effective ice thickness over the domain, calculated as the ice volume divided by the area of the domain. Hereafter, whenever ice thickness or volume is mentioned it

25   refers to these *effective* values, which includes the overlying snow as well.

The March ice area over the domain declines from a mean value of 9.3 x10^6 km^2 during the 1960-79 reference period, to 8.4 x10^6 km^2 towards the end of the 21st century (2090-2099) for the RCP2.6 scenario, and 5.2 x10^6 km^2 for the more aggressive RCP8.5 scenario (Fig. 3a). There is little divergence in the response of either the ice area or volume to the different forcing scenarios before about 2050 (Fig. 3), after which the stronger forcing scenarios show a greater loss of winter ice cover, with

30   RCP8.5 showing an especially steep decline from 2080 onwards. The mean March ice thickness over the domain declines from 2.3m during the period 1960 to 1979, to 1.2m during the 2090s for the RCP2.6 scenario, and 0.2m for RCP8.5.

For September, the mean ice area during the 1960-79 reference period is 4.1 x10^6 km^2, and the mean thickness is 1.5m. By the end of the 21st century, all the scenarios have less than 1.0 x10^6 km^2 of ice cover remaining in September, so that the Arctic Basin is virtually ice free.

3 Mean volume budget of the Arctic sea ice

5   The HadGEM2-ES model output includes sea ice volume tendencies due to thermodynamic and dynamic processes, and terms quantifying the thermodynamic processes acting on the ice and overlying snow. This allows us to construct a budget that balances the diagnosed changes in ice volume over any given period. In Keen et al (2013), the budget terms are expressed in terms of a heat anomaly per unit area of ice (in J m^{-2}). While this formulation enables an understanding of how the atmospheric and oceanic forcing of the ice is changing as the climate warms, the budget terms expressed this way cannot

10   be summed to balance the changes in the ice volume. Here we express the budget components in terms of their impact on the average ice thickness over the domain of Fig. 2, so the units are m of ice formed/lost. This is a similar formulation to that used by Holland et al (2010), although here we are also able to include individual components of the melt/freeze terms, and we also consider the seasonal cycle of the volume budget.

3.1 Mean volume budget for the reference period 1960-79

15   The components of the volume budget that we can diagnose for the HadGEM2-ES model are shown in Fig. 4, both as a decadal mean time series (for the RCP8.5 scenario) and as a mean seasonal cycle for the reference period 1960-79. As mentioned above, each component is expressed in terms of its impact on the ice thickness (averaged over the domain): a flux representing heat entering the ice will be shown as a negative value as it causes ice loss. We describe each component in turn:

20   •   Basal ice growth via the diffusive heat flux through the ice and snow (dark green lines) : In HadGEM2-ES, ice growth is dominated by basal ice formation due to the loss of heat via the diffusive heat flux through the ice and snow (Fig. 4a). This term is positive for most of the year (Fig. 4b), representing ice growth at the base of existing ice. The total amount of basal growth increases as ice forms during the autumn, and is a maximum during the winter. During the summer, this term can become small and negative (representing ice melt) when the surface

25   temperature rises about the freezing temperature of sea water (Fig. 4b).

    •   Basal melting due to heat from the ocean (light green lines): The ocean to ice heat flux is a function of the difference in temperature between the top layer of the ocean, and the temperature at the base of the ice (McPhee, 1992). It is maintained through diffusive and advective ocean processes, and melts ice at the bottom surface throughout the year, especially during the summer and autumn (Fig. 4b). This term is small and negative during the

winter, increasing in magnitude from April to a maximum in July, and then declines in magnitude through the late summer and autumn. In HadGEM2-ES this is the largest individual term causing ice melt (Fig. 4a).

- Top melting (dark blue lines): The top melting flux is the sum of the atmospheric turbulent and radiative heat fluxes, resulting in the surface melting of ice or snow. It is zero outside the melting season (Fig. 4b), and negative during the spring and early summer (as it causes ice melt). The amount of top melting peaks earlier in the melt season than the basal melting, and declines more quickly. In HadGEM2-ES there is less ice lost during the year by top melting than by basal melting (Fig. 4a).

- Advection (orange lines): The net impact of ice advection is to move ice out of the domain (to lower latitudes), and so this appears as a negative term in Fig. 4. There is a small seasonal cycle, with more ice lost by advection during the winter, falling from a monthly maximum of 2.8cm of ice loss during January, to 0.8cm by August. The amount of ice lost by advection each decade is smaller than the amount lost by either top or basal melting (Fig. 4a).

- Frazil ice formation (green/blue lines): This term represents the formation of ice in a grid box when the ocean temperature would otherwise fall below the freezing temperature. It is virtually zero during the summer, and a maximum in autumn (2.5cm of ice formation during November) as the ocean cools and the ice cover increases following its summer minimum. This component is always positive, as it solely represents ice formation.

- Snowfall (less sublimation) (red lines): This represents the snow accumulation due to snowfall, less any loss of ice or snow at the surface due to sublimation. It is positive in all months, a maximum during the winter (1.3cm of ice formation in December), and virtually zero during the summer melt season.

To summarise, in the decadal mean volume budget for HadGEM2-ES, ice growth is dominated by basal ice formation due to the diffusive heat flux through the snow and ice, which accounts for 85% of the annual mean ice formation during the reference period 1960-79, with smaller contributions due to frazil ice growth (7%) and the accumulation of snow (less sublimation) (7%). These processes are offset by melting at the base of the ice due to heat from the ocean (48% of annual mean ice loss) , melting at the top of the ice due to atmospheric fluxes (40%) , and ice advection out of the region (12%). The sum of these budget components (black line, Fig. 4a) is much smaller in magnitude than the individual components, representing the near balance between the processes of ice growth and loss, with the ice decline arising because of the small imbalance between these terms in the warming climate. This budget sum (Fig. 4a) matches the decadal changes in ice thickness

The HadGEM2-ES melting season extends from May to September during the 1960-79 reference period (Fig. 4b, solid black line), and during this time the melting is initially dominated by melting at the top surface of the ice, with basal melting due to heat from the ocean becoming more important later in the melt season, and continuing into the autumn. During the winter,

the dominant term is basal ice growth due to the diffusive heat flux. Note that ridging is not included in this decomposition, as it does not explicitly affect the ice volume: it changes the spatial distribution of ice within a grid box, but not the volume of the ice. That is not to say that the ridging is unimportant, merely that it has a null direct impact on the volume budget. In addition, lateral melting is not explicitly modelled in HadGEM2-ES and so does not appear in this decomposition, and as we

5 are considering the combined budget of the ice and overlying snow there is no snow-ice formation term.

4 Changes in the volume budget of the Arctic sea ice

Here we consider how the components in the volume budget change relative to the reference period 1960-79 discussed above, both in terms of their decadal evolution during the 21st century, and also how the seasonal cycle changes. Initially we focus on the strongest forcing scenario RCP8.5, and then we consider the impact of the different forcing scenarios on the

10 changes.

4.1 Results for the RCP8.5 forcing scenario

Figure 5 shows how the components of the volume budget change relative to the reference period 1960-79 for the RCP8.5 scenario. As the ice starts to decline, the ice loss initially results from a mean reduction in basal ice formation due to the diffusive heat flux through the ice (dark green line, Fig. 5b), and extra melting at the base of the ice due to heat from the

15 ocean (light green line). There is also a reduction in the accumulation of falling snow on the ice (red line). These changes are shown as negative values in Fig. 5, representing less ice growth (or more ice loss) relative to 1960-79. Offsetting these are a reduction in melting at the top surface of the ice due to atmospheric fluxes (dark blue line), reduced loss by advection (orange line), and more frazil ice formation (green/blue line).

These changes are similar to the response Holland et al (2010) found for our CMIP3 model HadGEM1 (their Fig. 7l), where

20 the volume decline was due to reductions in ice growth, offset by (smaller) decreases in ice melt and advective ice loss. This is not the case for all models though: Holland et al found that the CMIP3 models overall show a large model-to-model differences in the 21st century budget changes.

As the run progresses, the majority of these changes become more pronounced as the ice cover declines, the exceptions being the basal melting and the frazil ice formation (Fig. 5a). The amount of frazil ice formation initially increases (Fig. 5b),

25 then after 2010 it begin to decrease, until by the 2050s there is less frazil ice formation than during 1960-79 (Fig. 5a). The total amount of basal melting initially increases relative to 1960-79 (Fig. 5b), and then decreases from 2010 onwards, until by the 2040 there is less basal melt than there was during 1960-79 (Fig. 5a). In each case the reversal in sign is due to alterations in the balance between opposing changes that occur at different times of year, and is most easily understood by looking at changes in the seasonal cycles of the budget components (Fig. 6)

The budget changes causing extra net ice loss relative to 1960-79 occur at two distinct times of year: during May/June, and again during September-November (black line, Fig. 6a). These are partially offset by the changes occurring at other times of year, most notably during July and August.

Early in the melt season (May/June) there is extra ice loss due to top and basal ice melt, and also due to reduced basal ice
5 growth (Fig. 6a). During July and August there is less top melting and no extra basal melting, and so less net ice melt relative to the reference period. During the autumn, there is reduced basal ice formation, which becomes the largest budget change resulting in ice loss.

The changes shown in Fig. 6a are for the decade 2010-2019. Later in the integration (2040-49, Fig. 6b), changes in the budget components show broadly the same seasonal pattern as for the earlier decade, although the magnitude of the changes
10 relative to 1960-79 has increased as the ice area declines. The most notable differences are that by the 2040s the amount of basal melt in the late summer has reduced relative to the reference period, and that there is no net change in the amount of ice loss during June.

The amount of ice lost by advection is reduced at all times of year, and to a greater extent during the winter (orange line, Fig. 6). This is consistent with the reducing ice volume – there is less ice that can move out of the basin. In fact by the 2070s (not
15 shown), there is virtually no advective ice loss during August and September, consistent with the Arctic basin being almost completely free of ice by the end of the summer (Fig. 3).

There is reduced frazil ice formation in the autumn during the 2040s (Fig. 6b), and an increase in the winter months (November to March). The autumn change is consistent with warmer temperatures delaying the freeze-up, and the winter change is consistent with decreased ice cover exposing a larger area of ocean where frazil ice can form.

20 **4.2 Impact of the declining ice area on the volume budget**

The impact on the volume budget of the different processes acting on the ice and snow is strongly influenced by the ice area, and how it changes in response to the forcing scenario. For example the ice cover in September and October reduces more quickly in response to the forcing scenario than at other times of year (Fig. 7a), reducing the impact on the volume budget of changes occurring then. So while some of the changes in the budget components are clearly consistent with a warming
25 climate: for example the extra top and basal melting and reduced basal ice growth during the spring (Fig. 6), others have a less intuitive impact on the budget due to the declining ice cover.

In Fig. 7b, the dominant budget components have been weighted by the ice area to show how they change per unit area of ice. During the decade 2010-19 there is more melting at the ice surface during May/June relative to 1960-79: the warmer atmosphere leads to extra melting, enhanced by reductions in the surface albedo. For the remainder of the melt season there
30 is no extra surface melt, partly because by July the surface temperature is already close to the melting temperature during 1960-79, and hence there is little scope for further reductions in albedo. So during July and August the reduced ice area means that there is a smaller volume of ice lost by surface melt in 2010-19 (and later decades) relative to 1960-79 (Fig. 6).

There is more melting at the base of the ice throughout the melt season, especially during July, August and September (Fig. 7b), primarily due to the in-situ warming of the ocean surface as the ice cover retreats. In May and June this results in a greater volume of ice loss relative to 1960-79 (Fig. 6a). However due to the reduced ice area in the 2010s compared to the 1960s and 70s, the volume of ice lost by basal melt in the late summer is almost the same in each of the two time periods (Fig. 6a). Later in the integration, as the ice cover reduces further, there is less volume loss by basal melting in the late summer (Fig. 6b). This explains why the net impact of the ocean to ice heat flux changes sign during the model integrations (Fig. 5): the decadal timeseries initially only shows the impact of the extra basal melting that occurs during the spring, as there is little change at other times of year. As the forcing scenario progresses, the budget contribution due to reduced basal melting during the late summer starts to play a role, and towards the end of the 21st century it is this that dominates the decadal mean basal melt term.

Compared to 1960-79 there is more ice growth at the base of the ice during the autumn and winter, and less during the late summer for the decade 2010-19 (Fig. 7b). The diffusive heat flux causing the basal melt is a function of both the surface temperature and the ice thickness. In September the warmer temperatures in 2010-19 dominate, meaning reduced basal ice formation where there is still ice. There is a stronger dependence on the ice thickness at cooler temperatures, and from October onwards the fact that the ice is thinner in 2010-19 than during 1960-79 mean there is more diffusive heat loss to the atmosphere, and more ice formation at the base (Fig. 7b). However, the reductions in ice area during August, September and October mean that despite the extra growth over the remaining ice, a smaller volume of ice is formed at this time of year during 2010-19 than during 1960-79 (Fig. 6a).

In summary, for the HadGEM2-ES model the Arctic decline up to the 2020s for the RCP8.5 scenario is a result of reduced basal ice formation and extra basal melting, offset by reductions in melting at the top surface of the ice, and reduced advective ice loss. Later in the 21st century the total amount of basal melting decreases due to the shrinking ice area in the later summer, so that in the volume budget the basal melt term also offsets the reductions in basal ice growth.

4.3 Impact of forcing scenario

We now consider how the volume budget changes for the other forcing scenarios. Figure 8 shows changes in basal growth (relative to the reference period) for each of the four scenarios. All the scenarios show a decline in basal ice growth, with the more aggressive scenarios showing a greater decline. For the latter half of the 21st century there is a clear difference in response between RCP2.6, RCP4.5/6.0, and RCP8.5. For RCP2.6 the amount of basal ice growth levels off towards the end of the 21st century, consistent with the stabilisation of the ice area and volume in this scenario (Fig. 3), whereas for RCP6.0 the amount of basal growth continues to decline throughout the 21st century, albeit to a lesser extent than for the stronger RCP8.5 scenario (Fig. 8). A similar picture emerges for the other budget components (not shown): the signals of change for each scenario are broadly the same as already described for RCP8.5, although the exact timing and magnitude of the changes depends on the strength of the forcing.

By plotting the decadal response in each budget component as a function of decadal mean ice area rather than time (Fig. 9), we see that they each follow a common trajectory independent of the forcing scenario. Note that the plots in Fig 9 have different scales, as the intention here is to show the trajectory of each component, rather than their relative magnitudes. Hence changes in the volume budget components are independent of the speed at which the ice retreats, at least for the HadGEM2-ES model, and for the range of IPCC scenarios considered here. Figure 9 also confirms that the changes in the volume budget components are, as previously discussed, strongly dependent on the ice area.

Compared to the thermodynamic budget components, the changes due to advection are relatively small in relation to the inter-decadal variability of the control integration. By the end of the 21st century, the ratio between the response for scenario RCP8.5 and the variability in the control run is 6.8 for the advective term, whereas for the other budget terms this ratio ranges from 21.7 to 34.9.

We note that for most of the budget components the relationship with the ice area is non-linear. For example, when the annual mean ice area has reduced to approximately 6.5×10^6 km^2, the anomaly w.r.t 1960-79 in the total amount of frazil ice formation and basal melting changes sign, and the slope in the response of the basal ice formation steepens. This corresponds to the stage at which the Arctic basin first becomes seasonally ice-free, as shown in Fig. 10 where the budget components from Fig. 9 are plotted against the appropriate (10 year mean) September ice area. As the Arctic becomes seasonally ice-free, processes that were initially dominant in the ice volume budget during late summer/early autumn have a reduced impact on the decadal mean budget.

Although not shown here, the seasonal cycle of anomalies in the volume budget is also related to the remaining ice cover, and independent of the speed at which the ice retreated. For example, if we choose a decade for each of the scenarios with matching mean ice cover and over plot the anomalies they are very similar.

So in summary, while the strength of the forcing scenario affects the magnitude and timing of the decline in ice cover, for HadGEM2-ES the changes in the volume budget depend on the ice cover, and are independent of the speed at which the ice retreated.

5 Summary and discussion

We have investigated decadal changes in the seasonal cycle of the volume budget of the AR5 climate model HadGEM2-ES during the 21st century for a range of IPCC forcing scenarios. For this model, the processes that change most *at the ice surface* as the climate warms are top melting and basal melting during the summer and autumn. Extra top melting occurs during May and June, while basal melting due to extra heat from the warming ocean occurs from May onwards, reaching a peak in August and September. When the declining ice area is taken into account so that the budget terms can be summed to balance the actual changes in ice volume, we see that the decline in ice volume results primarily from reduced ice growth, offset by smaller reductions in ice melt and reduced advection to lower latitudes. The influence of the evolving ice area on 21st century changes in the sea ice has also been noted by Holland and Landrum (2015).

The seasonal cycle of the ice volume budget shows net ice loss in the spring and early summer due to extra surface and basal melting and reduced basal ice growth, and reduced basal growth during autumn/early winter. These changes are partially offset by net ice gain due to reduced amounts of surface melting during July and August as the ice cover declines.

The choice of forcing scenario affects the rate of ice decline and the timing of change in the volume budget components, but does not have a strong impact on the changes in the balance between the individual budget components, at least for the HadGEM2-ES model and for the range for forcing scenarios considered for IPCC AR5.

The budget changes shown here are likely to be dependent on the sea ice physics included in HadGEM2-ES. For example, the fact that the sea ice albedo is a function of surface temperature means that no further albedo reduction are possible once the surface temperature has reached the melting point, as happens in July for this model. A different behaviour may be seen in a model including an explicit representation of melt ponds. HadGEM2-ES uses zero-layer thermodynamics, which does not model the internal temperature of the ice, and has a constant ice salinity. A model including a multi-layer thermodynamic scheme and prognostic salinity might well show a greater sensitivity to the forcing scenario than we see for HadGEM2-ES.

The methodology used here should be readily applicable to other models, and in particular those with SIMIP diagnostics submitted to the CMIP6 data archive. Our results suggest that while it is useful to consider how budget components change over the ice surface, it is also beneficial to include the impact of the declining ice cover to generate a set of terms that can be summed to balance the actual changes in ice volume, as the different approaches can show a different balance between the budget terms, and the ice area itself affects the impact of each budget term. This will help to distinguish between the impact of changing processes acting at the ice surface and the impact of the loss of ice cover. This will be especially important if the CMIP6 models show as wide a spread in projected ice cover over the 21st century as the CMIP3 and CMIP5 models.

Competing interests. The authors declare no competing interests

Acknowledgements. This work was supported by the Joint UK BEIS/Defra Met Office Hadley Centre Climate Programme (GA01 101), and the European Union's Horizon 2020 Research & Innovation programme through grant agreement No. 727862 APPLICATE. The content of the paper is the sole responsibility of the authors and it does not represent the opinion of the European Commission, and the Commission is not responsible for any use that might be made of the information.

References

Caesar, J., Palin, E., Liddicoat, S., Lowe, J., Burke, E., Pardaens, A., Sanderson, M., and Kahana, R.: Response of the HadGEM2 earth system model to future greenhouse gas emissions pathways to the year 2300, J. Climate, 26(10), 3275–3284, doi:10.1175/jcli-d-12-00577.1, 2012

Collins, W. J., Bellouin, N., Doutriaux-Boucher, M., Gedney, N., Halloran, P., Hinton, T., Hughes, J., Jones, C. D., Joshi, M., Liddicoat, S., Martin, G., O'Connor, F., Rae, J., Senior, C., Sitch, S., Totterdell, I., Wiltshire, A., and Woodward, S.: Development and evaluation of an Earth-System model – HadGEM2. Geoscientific Model Development, 4(4), 1051–1075, doi:10.5194/gmd-4-1051-2011, 2011

5   Curry, J. A., Schramm, J. L., Perovich, D. K., and Pinto, J. O.: Applications of SHEBA/FIRE data to evaluation of snow/ice albedo parameterizations, J. Geophys. Res., 106(D14), 15345–15355, doi:10.1029/2000jd900311, 2001

English, J. M., Gettelman, A., and Henderson, G. R.: Arctic radiative fluxes: Present-Day biases and future projections in CMIP5 models, J. Climate, 28(15), 6019–6038, doi:10.1175/jcli-d-14-00801.1, 2015

Francis, J. A., Chan, W., Leathers, D. J., Miller, J. R., and Veron, D. E.: Winter northern hemisphere weather patterns
10   remember summer arctic sea-ice extent, Geophys. Res. Lett., 36(7), doi:10.1029/2009gl037274, 2009

Hibler, W. D.: A dynamic thermodynamic sea ice model, J. Phys. Oceanogr., 9(4), 815–846, doi:10.1175/1520-0485(1979)009\%3C0815:adtsim\%3E2.0.co;2. 1979

Holland, M., Serreze, M., and Stroeve, J.: The sea ice mass budget of the arctic and its future change as simulated by coupled climate models. Climate Dynamics, 34(2-3), 185–200, doi:10.1007/s00382-008-0493-4, 2010

15   Holland, M. M., and Landrum, L.: Factors affecting projected arctic surface shortwave heating and albedo change in coupled climate models, Phil. Trans. R. Soc. A, 373(2045), doi:10.1098/rsta.2014.0162, 2015

Holland, P. R., and Kimura, N.: Observed concentration budgets of arctic and antarctic sea ice, J. Climate, 29(14), 5241–5249, doi:10.1175/jcli-d-16-0121.1, 2016

Hunke, E. C., and Dukowicz, J. K.: An Elastic–Viscous–plastic model for sea ice dynamics. J. Phys. Oceanogr., 27(9),
20   1849–1867, doi:10.1175/1520-0485(1997)027\%3C1849:aevpmf\%3E2.0.co;2, 1997

Jahn, A., Kay, J. E., Holland, M. M., & Hall, D. M.: How predictable is the timing of a summer ice-free arctic? Geophys. Res. Lett., 43(17), URL doi:10.1002/2016gl070067, 2016

Jiang, J. H., Su, H., Zhai, C., Perun, V. S., Del Genio, A., Nazarenko, L. S., Donner, L. J., Horowitz, L., Seman, C., Cole, J., Gettelman, A., Ringer, M. A., Rotstayn, L., Jeffrey, S., Wu, T., Brient, F., Dufresne, J.-L., Kawai, H., Koshiro, T.,
25   Watanabe, M., LÉcuyer, T. S., Volodin, E. M., Iversen, T., Drange, H., Mesquita, M. D. S., Read, W. G., Waters, J. W., Tian, B., Teixeira, J., and Stephens, G. L.: Evaluation of cloud and water vapor simulations in CMIP5 climate models using NASA " A-Train" satellite observations. J. Geophys. Res., 117(D14), doi:10.1029/2011jd017237, 2012

Jones, C. D., Hughes, J. K., Bellouin, N., Hardiman, S. C., Jones, G. S., Knight, J., Liddicoat, S., O'Connor, F. M., Andres, R. J., Bell, C., Boo, K. O., Bozzo, A., Butchart, N., Cadule, P., Corbin, K. D., Doutriaux-Boucher, M., Friedlingstein, P., Gornall, J., Gray, L., Halloran, P. R., Hurtt, G., Ingram, W. J., Lamarque, J. F., Law, R. M., Meinshausen, M., Osprey, S., Palin, E. J., Parsons Chini, L., Raddatz, T., Sanderson, M. G., Sellar, A. A., Schurer, A., Valdes, P., Wood, N., Woodward, S., Yoshioka, M., and Zerroukat, M.: The HadGEM2-ES implementation of CMIP5 centennial simulations. Geoscientific Model Development, 4(3), 543–570, doi:10.5194/gmd-4-543-2011, 2011

Keen, A., Hewitt, H., and Ridley, J.: A case study of a modelled episode of low arctic sea ice, Clim Dyn, 41(5-6), 1229–1244, doi:10.1007/s00382-013-1679-y, 2013

Kwok, R., and Rothrock, D. A.: Decline in arctic sea ice thickness from submarine and ICESat records: 1958–2008, Geophys. Res. Lett., 36(15), doi:10.1029/2009gl039035, 2009

Lipscomb, W. H. : Remapping the thickness distribution in sea ice models. J. Geophys. Res., 106(C7), 13989–14000., doi:10.1029/2000jc000518, 2001

Lipscomb, W. H., and Hunke, E. C.: Modeling sea ice transport using incremental remapping. Mon. Wea. Rev., 132(6), 1341–1354., doi:10.1175/1520-0493(2004)132\%3C1341:msitui\%3E2.0.co;2, 2004

Martin, G. M., Bellouin, N., Collins, W. J., Culverwell, I. D., Halloran, P. R., Hardiman, S. C., Hinton, T. J., Jones, C. D., McDonald, R. E., McLaren, A. J., O'Connor, F. M., Roberts, M. J., Rodriguez, J. M., Woodward, S., Best, M. J., Brooks, M. E., Brown, A. R., Butchart, N., Dearden, C., Derbyshire, S. H., Dharssi, I., Doutriaux-Boucher, M., Edwards, J. M., Falloon, P. D., Gedney, N., Gray, L. J., Hewitt, H. T., Hobson, M., Huddleston, M. R., Hughes, J., Ineson, S., Ingram, W. J., James, P. M., Johns, T. C., Johnson, C. E., Jones, A., Jones, C. P., Joshi, M. M., Keen, A. B., Liddicoat, S., Lock, A. P., Maidens, A. V., Manners, J. C., Milton, S. F., Rae, J. G. L., Ridley, J. K., Sellar, A., Senior, C. A., Totterdell, I. J., Verhoef, A., Vidale, P. L., and Wiltshire, A.: The HadGEM2 family of met office unified model climate configurations. Geoscientific Model Development, 4(3), 723–757, doi:10.5194/gmd-4-723-2011, 2011

Maslanik, J., Stroeve, J., Fowler, C., and Emery, W.: Distribution and trends in arctic sea ice age through spring 2011. Geophys. Res. Lett., 38(13), doi:10.1029/2011gl047735, 2011

Massonnet, F., Fichefet, T., Goosse, H., Bitz, C. M., Philippon-Berthier, G., Holland, M. M., and Barriat, P. Y.: Constraining projections of summer arctic sea ice, The Cryosphere, 6(6), 1383–1394, doi:10.5194/tc-6-1383-2012, 2012

McLaren, A. J., Banks, H. T., Durman, C. F., Gregory, J. M., Johns, T. C., Keen, A. B., Ridley, J. K., Roberts, M. J., Lipscomb, W. H., Connolley, W. M., and Laxon, S. W.: Evaluation of the sea ice simulation in a new coupled atmosphere-ocean climate model (HadGEM1), J. Geophys. Res., 111(C12), doi:10.1029/2005jc003033, 2006

McPhee, M. G.: Turbulent heat flux in the upper ocean under sea ice, J. Geophys. Res., 97(C4), 5365–5379, doi:10.1029/92jc00239, 1992

Melia, N., Haines, K., and Hawkins, E.: Sea ice decline and 21st century trans-Arctic shipping routes. Geophys. Res. Lett., 43(18), doi:10.1002/2016gl069315, 2016

Moss, R. H., Edmonds, J. A., Hibbard, K. A., Manning, M. R., Rose, S. K., van Vuuren, D. P., Carter, T. R., Emori, S.,
Kainuma, M., Kram, T., Meehl, G. A., Mitchell, J. F. B., Nakicenovic, N., Riahi, K., Smith, S. J., Stouffer, R. J., Thomson,
5   A. M., Weyant, J. P., and Wilbanks, T. J.: The next generation of scenarios for climate change research and assessment.
Nature, 463(7282), 747–756, doi:10.1038/nature08823, 2010

Notz, D.: How well must climate models agree with observations? Phil. Trans. R. Soc. A, 373(2052),
doi:10.1098/rsta.2014.0164, 2015

Notz, D., Jahn, A., Holland, M., Hunke, E., Massonnet, F., Stroeve, J., Tremblay, B., and Vancoppenolle, M.: The CMIP6
10 Sea-Ice model intercomparison project (SIMIP): understanding sea ice through climate-model simulations. Geoscientific
Model Development, 9(9), 3427–3446, doi:10.5194/gmd-9-3427-2016, 2016

Overland, J. E., and Wang, M.: Large-scale atmospheric circulation changes are associated with the recent loss of arctic sea
ice. Tellus A: Dynamic Meteorology and Oceanography, 62(1), 1–9, doi:10.1111/j.1600-0870.2009.00421.x, 2010

Post, E., Bhatt, U. S., Bitz, C. M., Brodie, J. F., Fulton, T. L., Hebblewhite, M., Kerby, J., Kutz, S. J., Stirling, I., and
15 Walker, D. A.: Ecological consequences of Sea-Ice decline. Science, 341(6145), 519–524, doi:10.1126/science.1235225,
2013

Rampal, P., Weiss, J., and Marsan, D.: Positive trend in the mean speed and deformation rate of arctic sea ice, 1979–2007. J.
Geophys. Res., 114(C5), doi:10.1029/2008jc005066, 2009

Semtner, A. J.: A model for the thermodynamic growth of sea ice in numerical investigations of climate. J. Phys. Oceanogr.,
20 6(3), 379–389, doi:10.1175/1520-0485(1976)006\%3C0379:amfttg\%3E2.0.co;2, 1976

Serreze, M. C., and Stroeve, J.: Arctic sea ice trends, variability and implications for seasonal ice forecasting. Phil. Trans. R.
Soc. A, 373(2045), doi:10.1098/rsta.2014.0159, 2015

Spreen, G., Kwok, R., and Menemenlis, D.: Trends in arctic sea ice drift and role of wind forcing: 1992–2009. Geophys.
Res. Lett., 38(19), doi:10.1029/2011gl048970, 2011

25 Stroeve, J. C., Kattsov, V., Barrett, A., Serreze, M., Pavlova, T., Holland, M., and Meier, W. N. : Trends in arctic sea ice
extent from CMIP5, CMIP3 and observations. Geophys. Res. Lett., 39(16), doi:10.1029/2012gl052676, 2012

Thorndike, A. S., Rothrock, D. A., Maykut, G. A., & Colony, R.: The thickness distribution of sea ice. J. Geophys. Res.,
80(33), 4501–4513, doi: 10.1029/jc080i033p04501, 1975

Uotila, P., Holland, P. R., Vihma, T., Marsland, S. J., & Kimura, N.: Is realistic antarctic sea-ice extent in climate models the
30 result of excessive ice drift? Ocean Modelling, 79, 33–42, doi:10.1016/j.ocemod.2014.04.004, 2014

Wang, M., and Overland, J. E.: A sea ice free summer arctic within 30 years? Geophys. Res. Lett., 36(7), doi:10.1029/2009gl037820, 2009

West A. E., Collins M., Blockley E., Ridley J., Bodas-Salcedo A.: Understanding Arctic sea ice biases in a climate model in conjunction with surface radiation biases. In preparation.
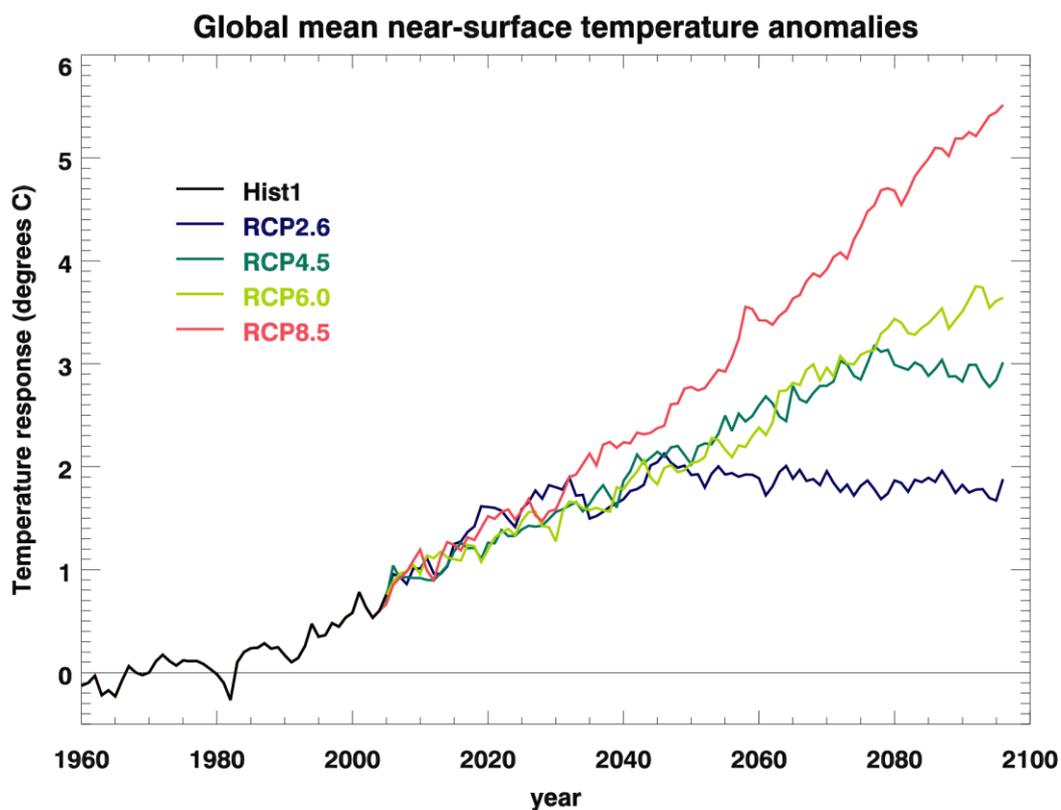
Figure 1: Global mean near-surface air temperature anomalies for HadGEM2ES for the IPCC CMIP5 Historical forcing scenario (black), followed by RCP8.5 (red), RCP6.0 (light green), RCP4.5 (dark green), and RCP2.6 (blue); the 1st ensemble member in each case.
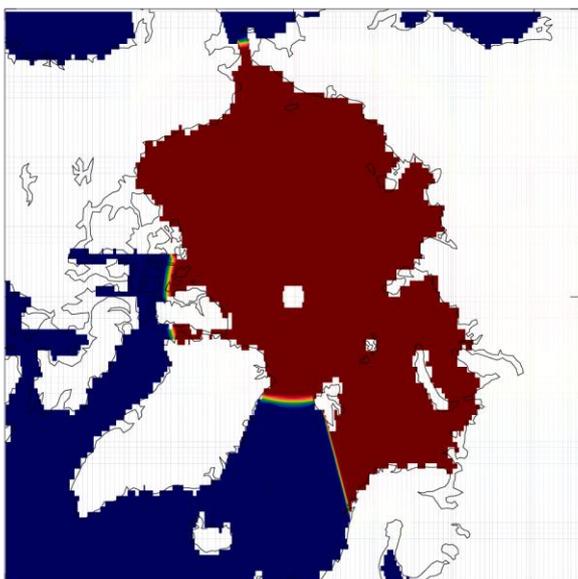
Figure 2: Definition of the Arctic region used in the analysis.
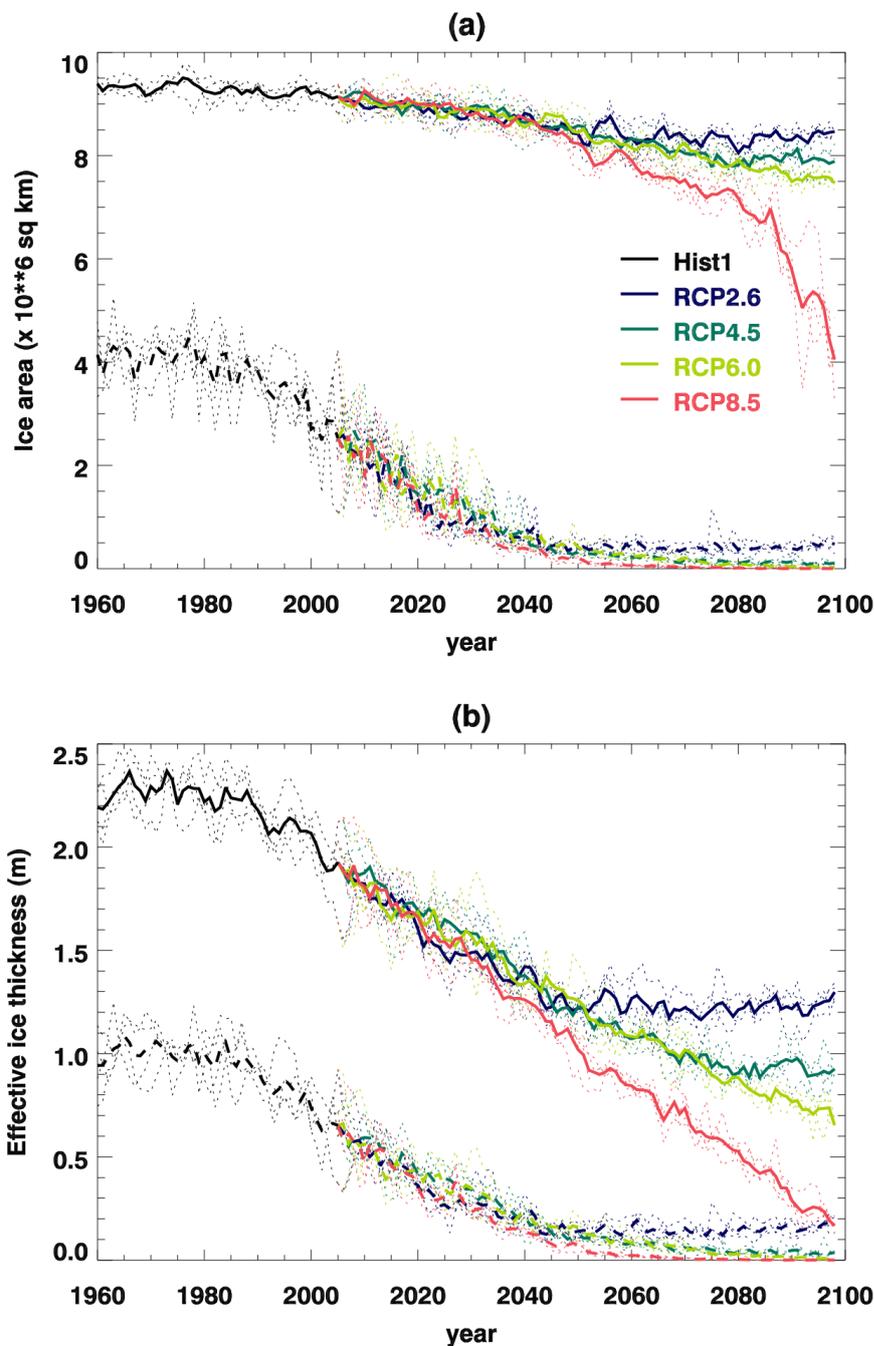
Figure 3: Evolution of (a) the ice area and (b) the mean effective ice thickness for March (solid lines) and September (dash lines) over the region defined in Fig. 2, for each of the HadGEM2-ES integrations. Bold lines show the ensemble means, and dotted lines show the individual ensemble members in each case.
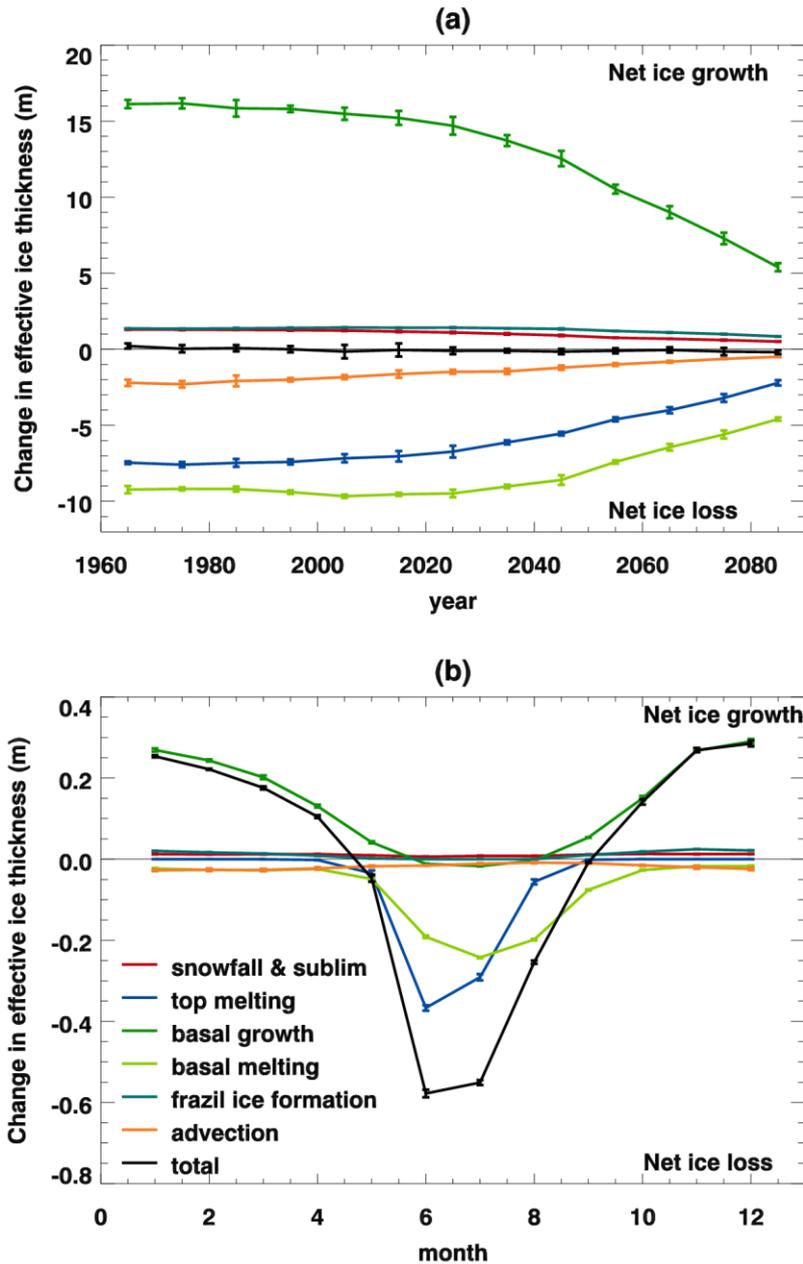
Figure 4: Components of the sea ice volume budget as defined in section 3.1 for the HadGEM2-ES Hist+RCP8.5 integrations, averaged over the region defined in Fig. 2. Values are ensemble means +/- 1 standard deviation, and positive values correspond to net ice growth.

(a) Decadal mean timeseries.

(b) Seasonal cycle for the reference period 1960-79.
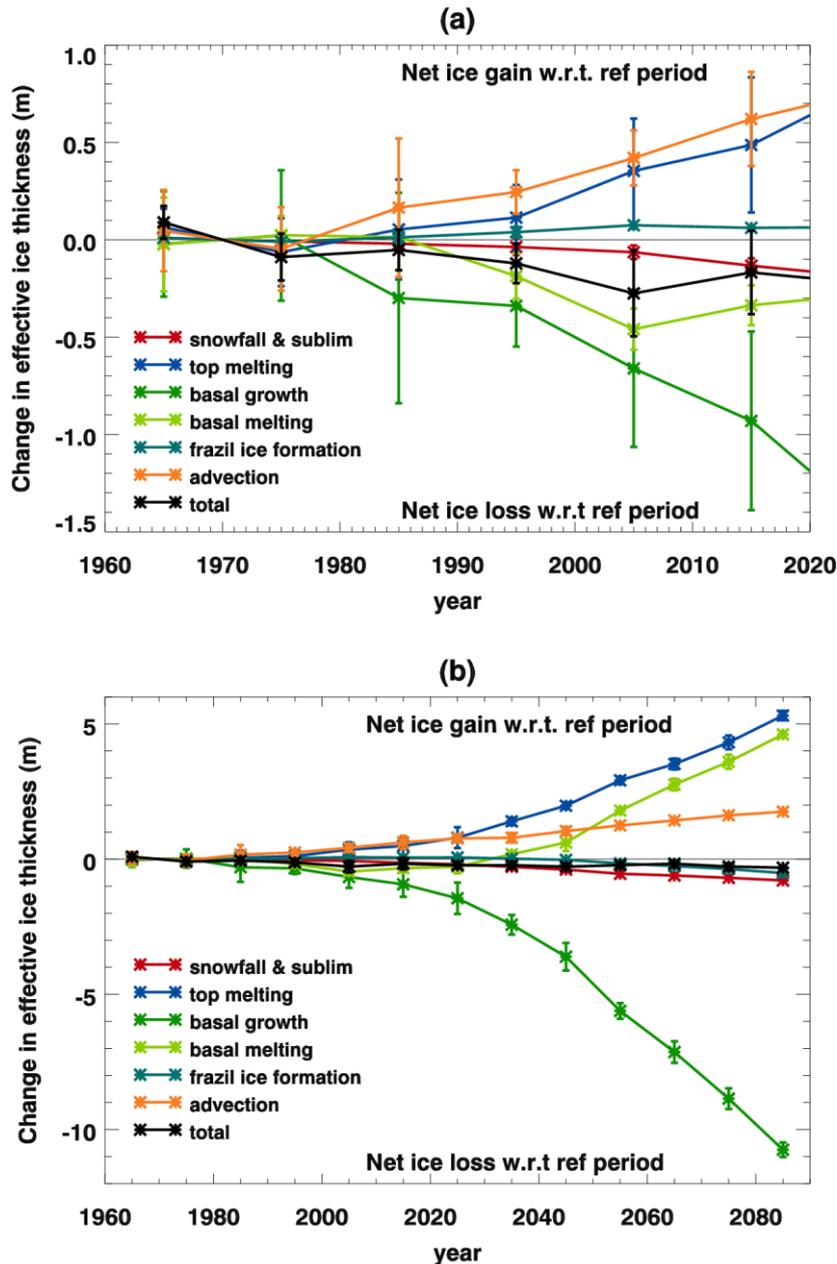
Figure 5: Decadal mean components of the sea ice volume budget as defined in section 3.1 for the HadGEM2-ES
Hist+RCP8.5 integrations, averaged over the region defined in Fig. 2 and plotted as differences relative to the mean over the
reference period 1960-79. Values are ensemble means +/- 1 standard deviation, and positive values correspond to net ice

5 gain w.r.t. the reference period.

(a) To 2020 (with expanded vertical scale)   (b) To 2090
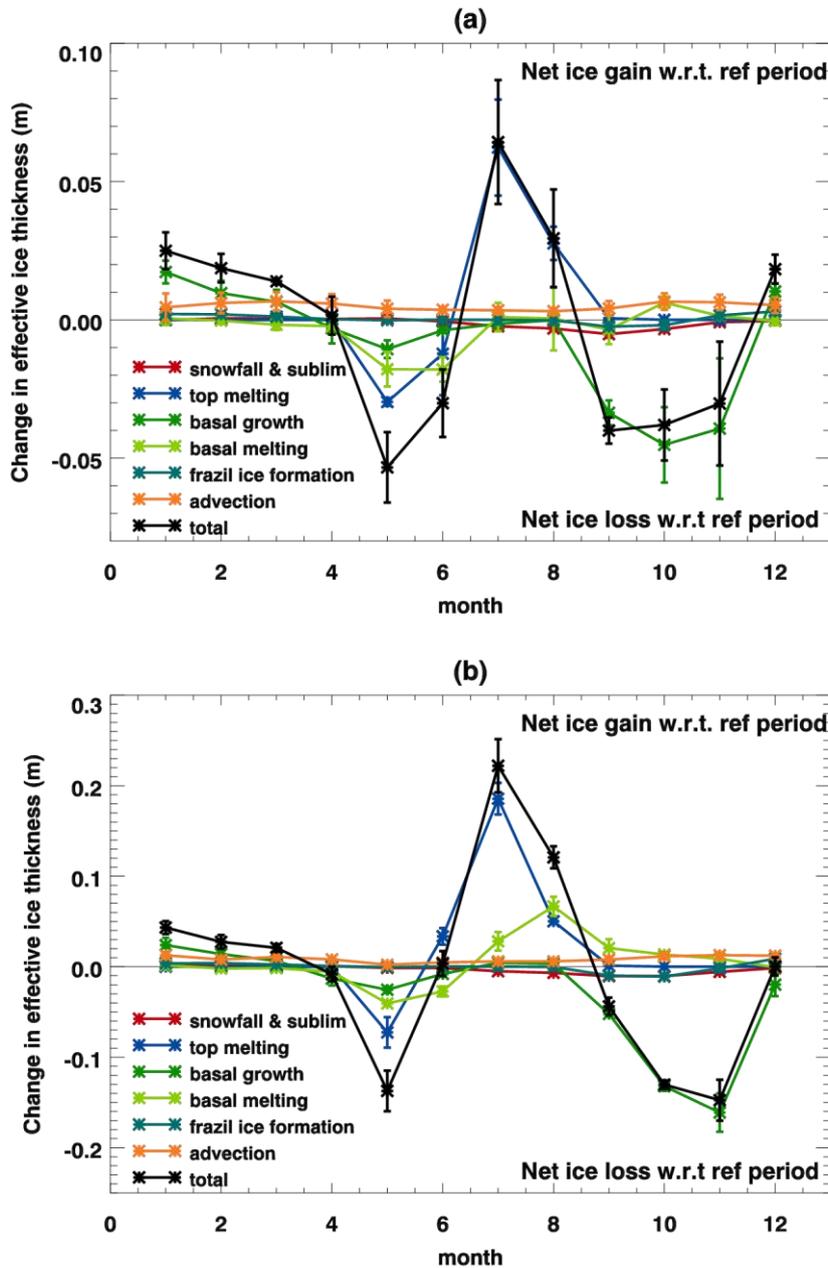
Figure 6: Ensemble mean seasonal cycles of the sea ice volume budget components as defined in section 3.1 for the HadGEM2-ES Hist+RCP8.5 integrations, averaged over the region defined in Fig. 2 and plotted as differences relative to the mean over the reference period 1960-79. Values are ensemble means +/- 1 standard deviation, and positive values correspond to net ice gain w.r.t. the reference period. (a) 2010-2019 (b) 2040-49. Note that the plots have different vertical scales.
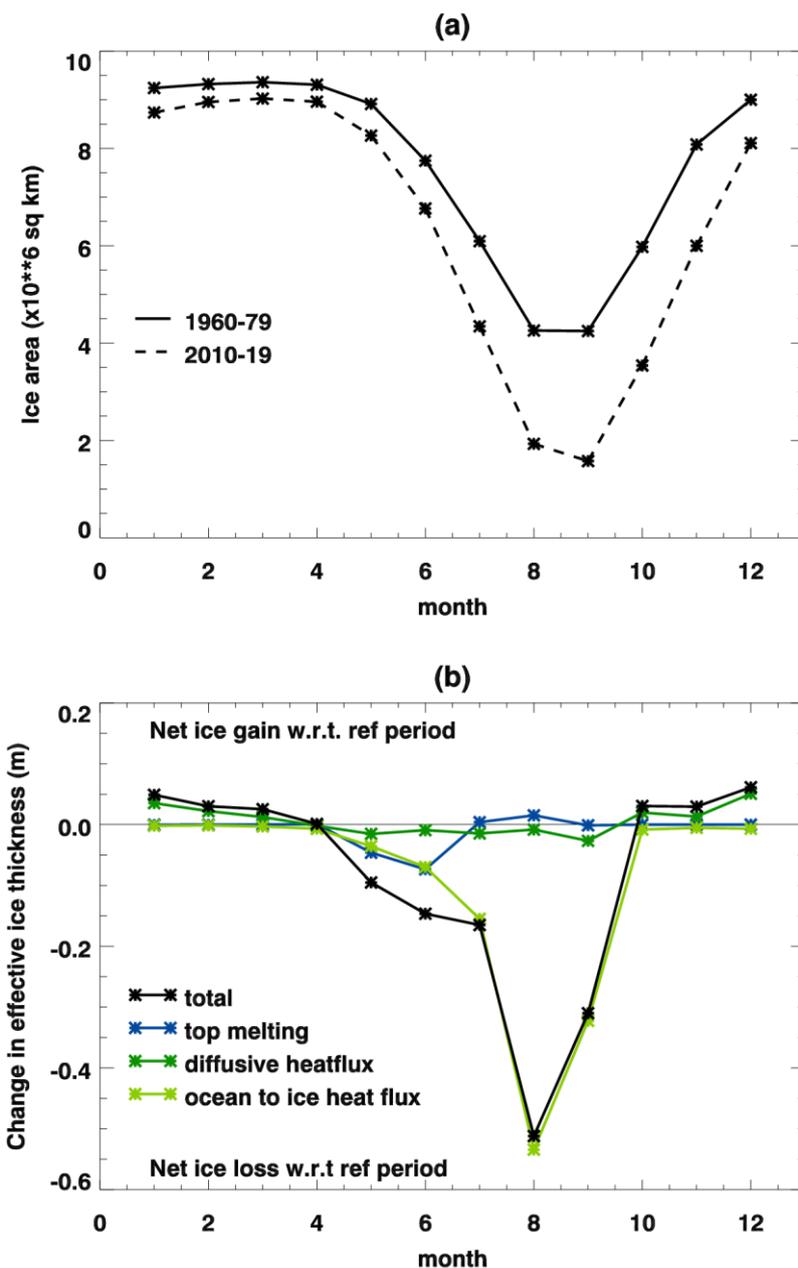
Figure 7: (a) Ice area over the domain defined in Fig. 2 for the reference period 1960-79 and for 2010-19 for the HadGEM2-ES Hist1+RCP8.5 scenario. (b) Seasonal cycles of selected sea ice volume budget components as defined in section 3.1 for the HadGEM2-ES Hist1+RCP8.5 integration, averaged over the region defined in Fig. 2 and plotted as differences relative to the mean over the reference period 1960-79, weighted by the ice area in each case, so that the change is per unit area of the remaining ice.
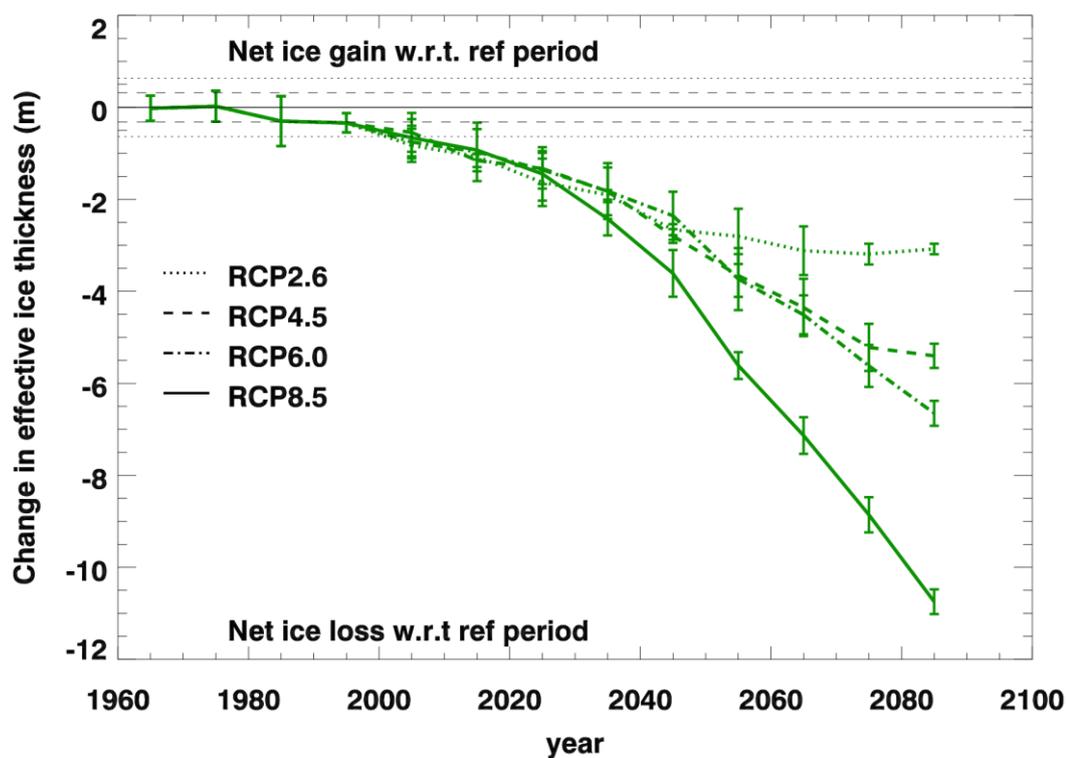
Figure 8: Decadal mean values of the basal growth component of the sea ice volume budget of HadGEM2-ES, plotted as differences relative to the reference period 1960-79, for each of the forcing scenarios. Values are ensemble means +/- 1 standard deviation, and positive values correspond to net ice gain w.r.t. the reference period. The dash and dot lines show +/- 1 and 2 standard deviations as calculated from 250 years of the HadGEM2-ES pre-industrial control integration.
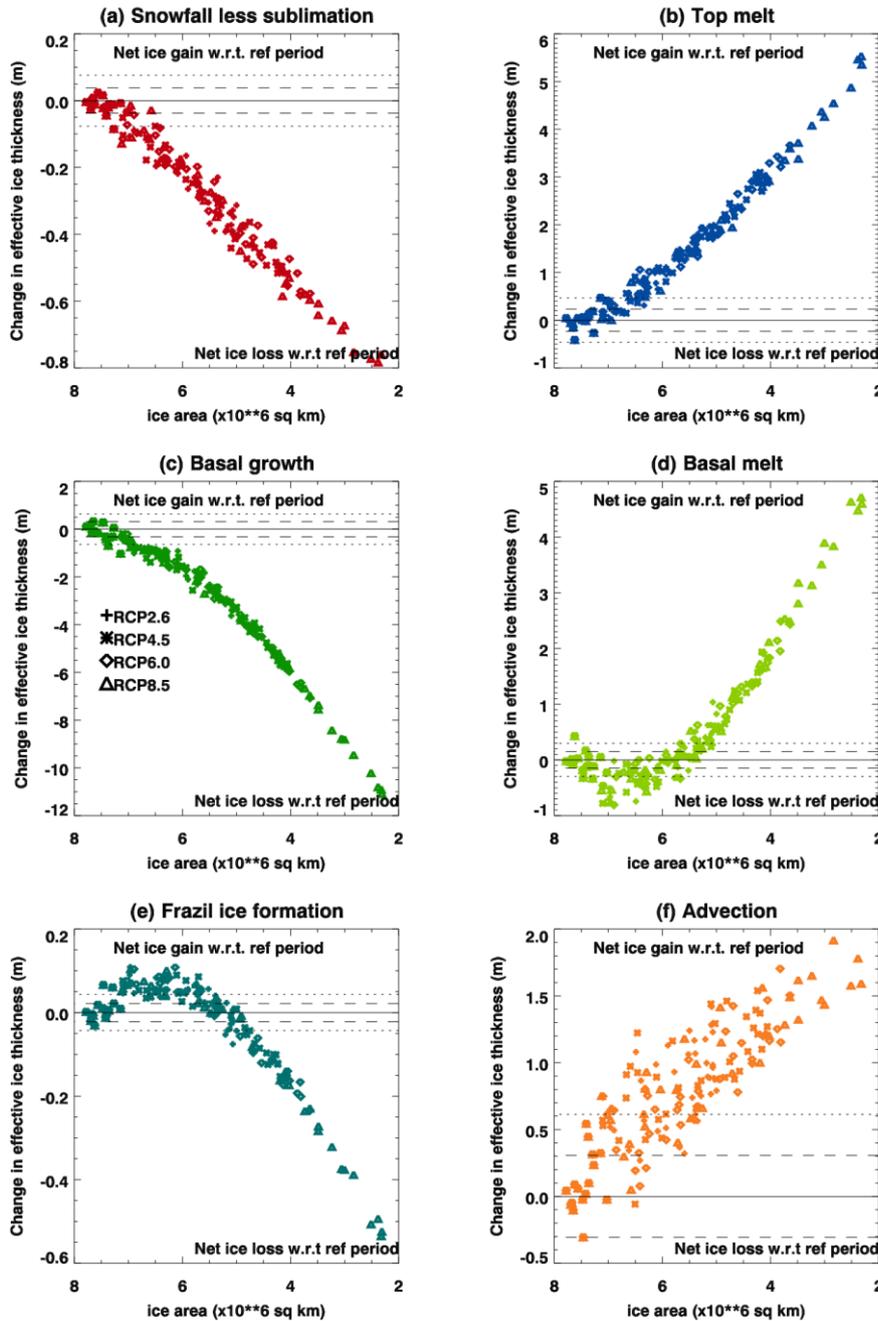
Figure 9: Decadal mean sea ice volume budget components for HadGEM2-ES all the forcing scenarios plotted as differences relative to the reference period 1960-9, and as a function of the decadal mean ice area. Positive values correspond to net ice gain relative to the reference period. The dash and dot lines show +/- 1 and 2 standard deviations as calculated from 250 years of the HadGEM2-ES pre-industrial integration. Note that the plots have different vertical scales.
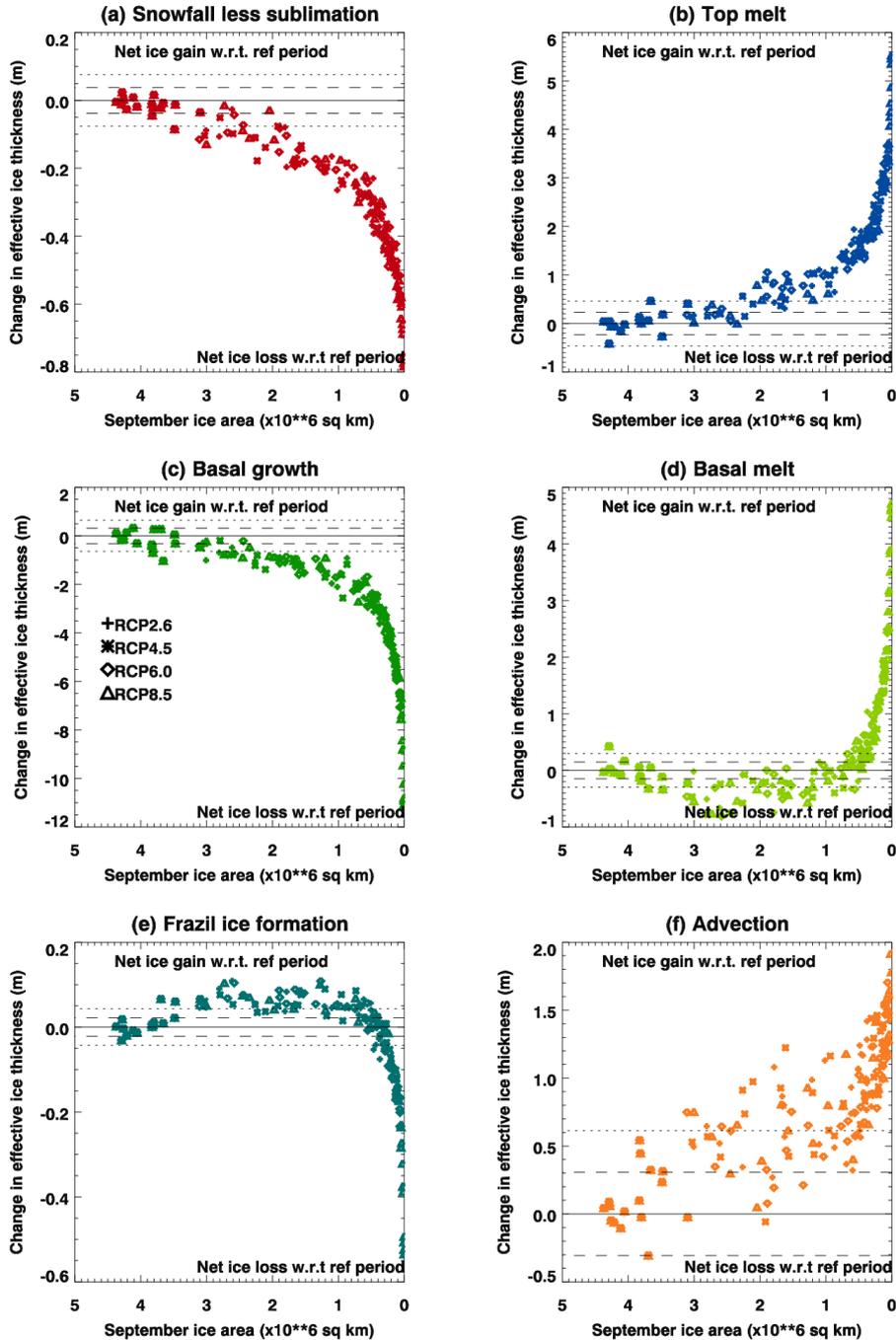
Figure 10: As figure 9, but plotted against decadal mean September ice area rather than the decadal mean over all months.